RESEARCH ARTICLE

Reelin and CXCL12 regulate distinct migratory behaviors during the development of the dopaminergic system

Gabriela Oana Bodea[1], Jan-Hendrik Spille[2], Philipp Abe[3], Aycan Senturk Andersson[4,5], Amparo Acker-Palmer[4,5], Ralf Stumm[3], Ulrich Kubitscheck[2] and Sandra Blaess[1,*]

ABSTRACT

The proper functioning of the dopaminergic system requires the coordinated formation of projections extending from dopaminergic neurons in the substantia nigra (SN), ventral tegmental area (VTA) and retrorubral field to a wide array of forebrain targets including the striatum, nucleus accumbens and prefrontal cortex. The mechanisms controlling the assembly of these distinct dopaminergic cell clusters are not well understood. Here, we have investigated in detail the migratory behavior of dopaminergic neurons giving rise to either the SN or the medial VTA using genetic inducible fate mapping, ultramicroscopy, time-lapse imaging, slice culture and analysis of mouse mutants. We demonstrate that neurons destined for the SN migrate first radially and then tangentially, whereas neurons destined for the medial VTA undergo primarily radial migration. We show that tangentially migrating dopaminergic neurons express the components of the reelin signaling pathway, whereas dopaminergic neurons in their initial, radial migration phase express CXC chemokine receptor 4 (CXCR4), the receptor for the chemokine CXC motif ligand 12 (CXCL12). Perturbation of reelin signaling interferes with the speed and orientation of tangentially, but not radially, migrating dopaminergic neurons and results in severe defects in the formation of the SN. By contrast, CXCR4/CXCL12 signaling modulates the initial migration of dopaminergic neurons. With this study, we provide the first molecular and functional characterization of the distinct migratory pathways taken by dopaminergic neurons destined for SN and VTA, and uncover mechanisms that regulate different migratory behaviors of dopaminergic neurons.

KEY WORDS: Dopaminergic neurons, Ventral midbrain, Tangential migration, Reelin, Chemokine

INTRODUCTION

Neuronal migration is one of the fundamental mechanisms establishing the complex organization of the brain. Migratory behavior and the underlying molecular mechanisms have been extensively studied in the dorsal brain, particularly in the cerebral and cerebellar cortex, where neurons undergo either radial or tangential migration to organize themselves into neuronal layers

[1]Institute of Reconstructive Neurobiology, Life and Brain Center, University of Bonn, Sigmund-Freud-Strasse 25, 53127 Bonn, Germany. [2]Institute of Physical and Theoretical Chemistry, University of Bonn, Wegelerstrasse 12, 53115 Bonn, Germany. [3]Institute of Pharmacology and Toxicology, Jena University Hospital, Friedrich Schiller University Jena, Drackendorfer Strasse 1, 07747 Jena, Germany. [4]Institute of Cell Biology and Neuroscience and Buchmann Institute for Molecular Life Sciences (BMLS), Goethe University Frankfurt, Max-von-Laue-Strasse 15, 60438 Frankfurt am Main, Germany. [5]Focus Program Translational Neurosciences (FTN), University of Mainz, Langenbeckstrasse 1, 55131 Mainz, Germany.

*Author for correspondence (sblaess@uni-bonn.de)

(Chédotal, 2010; Marín et al., 2010). By contrast, neurons in ventral brain areas are arranged into a complex array of neuronal clusters, so-called nuclei. Little is known about the migration events and the molecular mechanism that guide neurons to form these neuronal clusters.

Dopaminergic (DA) neurons in the ventral midbrain are organized into three major nuclei: the lateral substantia nigra pars compacta (SN), the medially located ventral tegmental area (VTA) and the posterolaterally located retrorubral field (RRF). The SN projects to the dorsal striatum and modulates motor behaviors. The VTA projects to corticolimbic targets and is important for reward behavior and the modulation of cognition, whereas the RRF projects to the ventrolateral striatum (Björklund and Dunnett, 2007; Ikemoto, 2007). DA neurons are of clinical interest as the degeneration of SN neurons underlies the major symptoms in Parkinson's disease. Dopamine imbalances in the corticolimbic system, which receives inputs from the VTA, have been linked to attention deficit hyperactivity disorder, addiction and schizophrenia (Dailly et al., 2004; Sulzer, 2007; Winterer and Weinberger, 2004; Wise, 2009).

DA neurons arise from progenitors in the midbrain floor plate that express sonic hedgehog (SHH), forkhead box A1 and A2 (FOXA1/2) and LIM homeobox transcription factor 1 alpha and beta (LMX1A/B) (Ang, 2009; Blaess et al., 2011; Chung et al., 2009; Hayes et al., 2011; Joksimovic et al., 2009; Nakatani et al., 2010; Yan et al., 2011). The induction of these factors requires SHH signaling and, accordingly, DA progenitors express GLI1, a readout for SHH signaling, prior to the onset of SHH expression (Andersson et al., 2006; Blaess et al., 2011; Hayes et al., 2011). Moreover, a subset of DA progenitors is positive for WNT1 (wingless-related MMTV integration site 1) (Brown et al., 2011).

The first differentiated DA neurons appear between embryonic day (E) 10.5 and E11.5 (Bayer et al., 1995). DA neurons migrate from their ventral midline progenitor area to the mantle layer, where they settle in distinct clusters to form the SN, VTA or RRF. Two distinct migration models, based primarily on immunostaining for tyrosine hydroxylase (TH), the rate limiting enzyme in dopamine synthesis and/or birthdating of ventral midbrain cells, have been put forward: (1) VTA and SN are primarily formed through radial migration (Hanaway et al., 1971), (2) DA neurons initially migrate radially towards the pial surface and then tangentially to form the VTA and SN (Kawano et al., 1995; Marchand and Poirier, 1983; Shults et al., 1990; Vasudevan et al., 2012). These studies could not unambiguously distinguish between different DA subpopulations during their migration phase nor did they monitor migratory behavior in real time. Therefore, it remains unclear which of these proposed migration paths are taken by DA neurons and whether DA neurons giving rise to the SN, VTA or RRF show distinct migratory behaviors. Markers that are expressed specifically in SN, VTA or RRF neurons throughout their development have not been identified, hampering the characterization of distinct DA migratory paths and

the identification of the molecular mechanisms that regulate DA neuronal migration. Based on loss-of-function mouse mutants in which the formation of the SN and/or VTA is impaired, only the netrin receptor DCC (deleted in colorectal carcinoma), the extracellular glycoprotein reelin, and the cell adhesion molecule L1 (L1CAM – Mouse Genome Informatics) have been implicated in the regulation of DA neuronal migration (Ballmaier et al., 2002; Demyanenko et al., 2001; Kang et al., 2010; Nishikawa et al., 2003).

Here, we show that cells destined for both the SN and the VTA migrate radially from the progenitor domain to the forming mantle layer, resulting in the intermingling of the two DA populations in the medial ventral midbrain at early differentiation stages. The separation of the distinct populations occurs through tangential migration of cells destined for the SN. We demonstrate that reelin signaling specifically regulates tangential migration of DA neurons whereas signaling through CXCR4, a receptor for the chemokine CXCL12, modulates the radial migration of DA neurons.

RESULTS
Fate-mapping strategy to follow the migration of DA neurons contributing to the SN or medial VTA
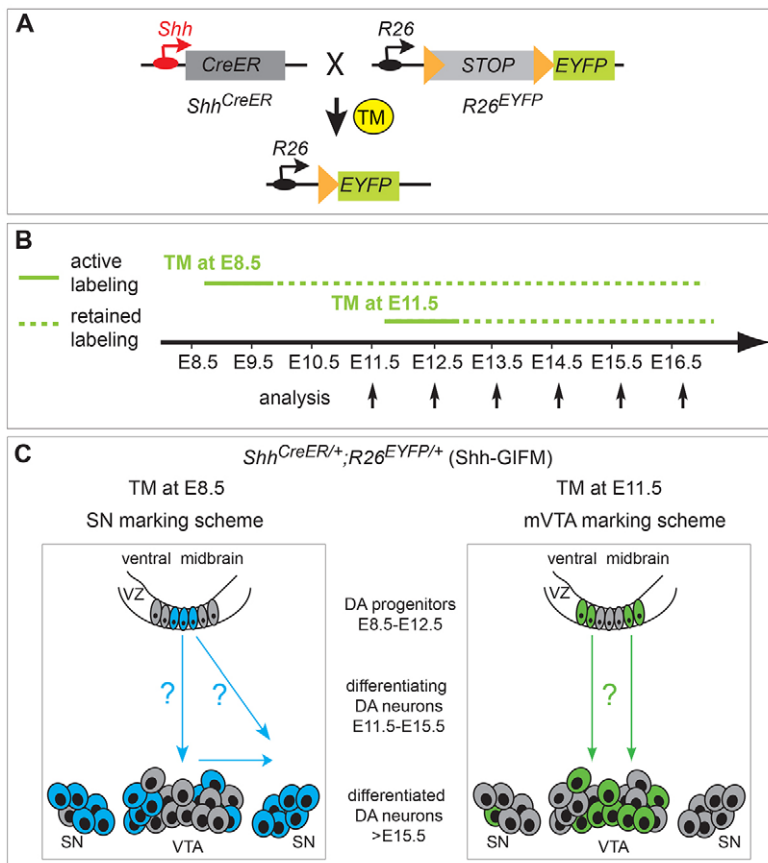
Using genetic inducible fate mapping, which heritably marks progenitors and their descendants, we and others have shown that SHH-expressing progenitors in the floor plate give rise to DA neurons. SHH is expressed in DA progenitors in the medial floor plate between E8.5 and E9.0, but at E11.5 it is excluded from the medial domain and restricted to lateral DA progenitors (Blaess et al., 2011; Hayes et al., 2011; Joksimovic et al., 2009). When genetic fate mapping of SHH-expressing cells is induced at E8.5, medial DA progenitors and their descendants are marked; these cells show a biased contribution to the SN (SN marking scheme). Induction at

E11.5 marks lateral DA progenitors and their descendants; this population contributes preferentially to the medial VTA consisting of the paranigral and interfasicular nucleus (mVTA marking scheme) (Fig. 1). Progenitor populations labeled with the SN or mVTA marking scheme also give rise to neurons in the lateral VTA (parabrachial nucleus) and to a few cells in the mVTA or SN, respectively (Blaess et al., 2011; Hayes et al., 2011; Joksimovic et al., 2009). Nevertheless the two populations are sufficiently distinct to examine separately the migratory routes and behavior of DA neurons contributing to the SN or the mVTA (Fig. 1C). To achieve fluorescent labeling of fate-mapped cells, we used an EYFP reporter allele ($R26^{EYFP}$) (Srinivas et al., 2001) (Fig. 1A).

Distribution of DA neurons destined for the SN shifts from medial to lateral during embryonic development

To identify fate-mapped, differentiated DA neurons, we performed immunostaining for TH and EYFP. We used this double-labeling approach because, in addition to DA progenitors and DA neurons, some non-DA neurons are labeled with the SN and mVTA marking scheme in the ventral midbrain (Blaess et al., 2011). Quantification of EYFP positive (EYFP^{pos}) and TH^{pos}/EYFP^{pos} cells at E13.5 and E14.5 showed that within the areas that contain differentiated DA neurons, >70% of EYFP^{pos} cells were also TH^{pos} (supplementary material Fig. S1).

To investigate the migratory routes of DA neurons, we characterized the distribution of DA neurons labeled with the SN or mVTA marking scheme (TH^{pos}/EYFP^{pos}) at three levels along the anteroposterior axis of the developing ventral midbrain (referred to as anterior, intermediate and posterior) between E11.5 and E16.5 (Figs 2, 3; supplementary material Fig. S2). From anterior to posterior, these areas correspond to the following DA nuclei in the

Fig. 1. Genetic inducible fate mapping (GIFM) of DA neurons in the ventral midbrain. (A) GIFM provides temporal and spatial control of cell marking through an inducible form of a site-specific recombinase, CreER, and a reporter allele such as ROSA$^{loxP-STOP-loxP-EYFP}$ ($R26^{EYFP}$), which permanently expresses EYFP upon Cre-mediated recombination. Temporal control of marking is achieved by tamoxifen (TM) administration at specific stages to activate CreER. Spatial control is attained by expressing CreER from the endogenous Shh locus (Shh^{CreER}). Orange triangles represent loxP sites. (B) CreER activation occurs several hours after TM administration and is maintained for ~24 hours (active labeling). Once Cre-mediated recombination occurs, the cell labeling is retained (retained labeling). (C) GIFM of Shh-expressing cells. TM administration at E8.5 (TM at E8.5) labels medial DA progenitors that have a biased contribution to SN neurons (SN marking scheme). TM at E11.5 labels lateral DA progenitors that preferentially give rise to mVTA neurons (mVTA marking scheme). Note that GIFM results in mosaic labeling; only a subset of cells is recombined within a given SHH-expressing progenitor domain. Arrows indicate potential migration paths of DA neurons.
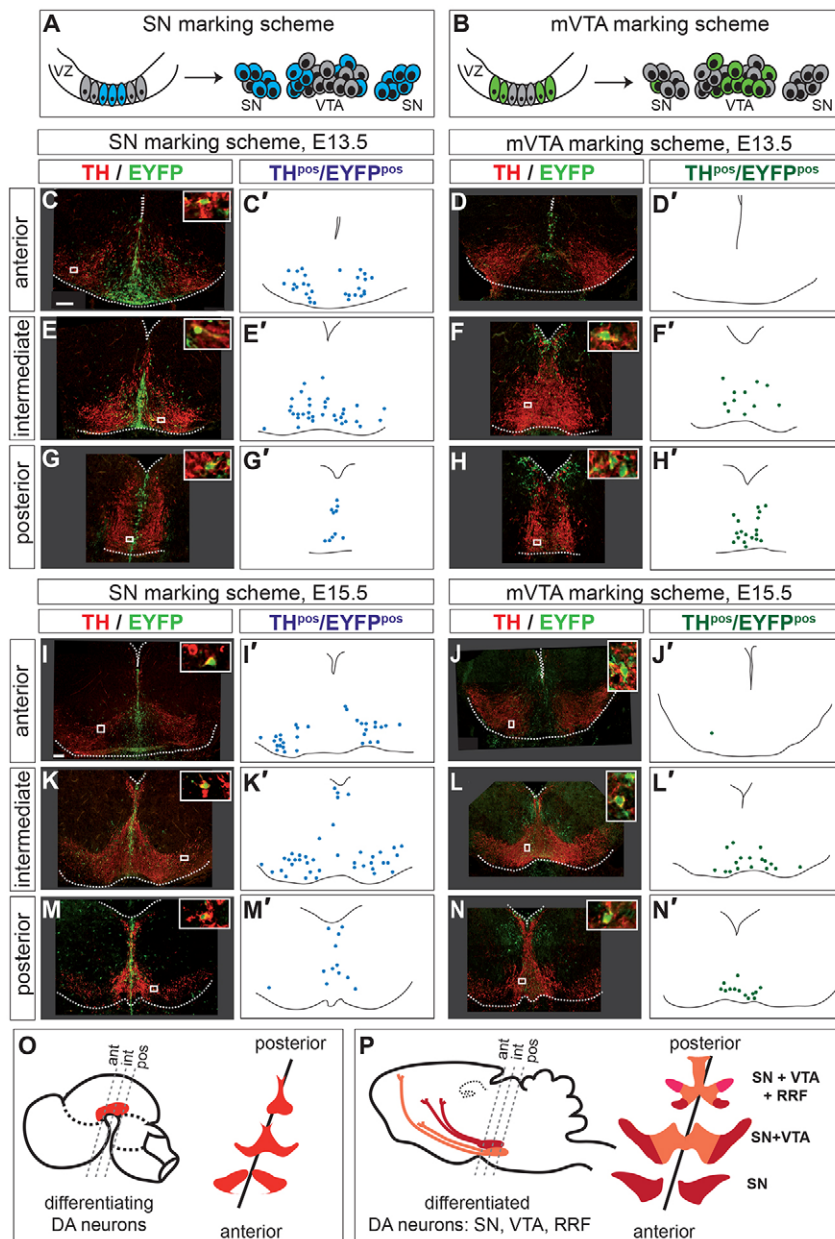
Fig. 2. Distinct distribution of DA neurons destined for the SN or mVTA in the developing midbrain. (A,B) SN or mVTA marking scheme. (C-N) E13.5 (C-H) and E15.5 (I-N) coronal sections at three anteroposterior levels were immunostained for TH and EYFP to visualize fate-mapped DA neurons. The ventricle and the pial surface are outlined. Insets show higher magnification of the boxed areas. (C′-N′) Representative schematics showing the distribution of fate-mapped cells (TH^{pos}/EYFP^{pos}, indicated by blue or green dots). Note that images/schematics at E13.5 and E15.5 are not to scale. (O) The plane of section shown in C-N. Red, DA neuron-containing area. (P) The corresponding levels in the adult brain. Scale bar: 100 μm.

adult brain: anterior SN; intermediate SN and anterior VTA; posterior SN, posterior VTA and RRF (Fig. 2P). Fig. 2 shows examples of the distribution of the fate-mapped DA-neurons at E13.5 and E15.5. To quantify the mediolateral position of the fate-mapped DA neurons, we determined the ventral midline in each section and divided the ventral midbrain into bins of 100 μm along the mediolateral axis (Fig. 3A-D). The number of fate-mapped DA neurons per bin was counted and expressed as percentage of the total number of fate-mapped DA neurons per section (Fig. 3E,F). At intermediate and posterior levels, DA neurons labeled with both marking schemes were found close to the midline (0-300 μm) between E11.5 and E13.5 (Fig. 2E-H; Fig. 3A,C,E,F; supplementary material Fig. S2B-D). At later stages (E15.5-E18.5), DA neurons labeled with the SN marking scheme were located in increasingly more lateral positions, whereas DA neurons labeled with the mVTA marking scheme maintained a relative medial position (0-400 μm) (Fig. 2K-N; Fig. 3B,D-F; supplementary material Fig. S2B,C). At anterior levels, DA neurons labeled with the SN marking scheme

were lateral to the midline by E11.5 and were observed in increasingly lateral positions at subsequent stages (Fig. 2C,I; supplementary material Fig. S2A,D). The mVTA marking scheme labeled only a few DA neurons in anterior sections (Blaess et al., 2011) (Fig. 2D,J).

In summary, DA neurons destined for the SN and mVTA were intermingled in the medial mantle layer between E12.5 and E13.5 and only separated later (E14.5-E15.5) into two largely distinct clusters. These results suggest that all DA neurons initially migrate radially from the ventricular zone to the mantle layer, and that neurons forming the SN undergo active tangential migration to reach their final lateral position.

DA neurons giving rise to the SN have tangentially oriented leading processes
On a cellular level, the process of migration consists of three steps: the extension of a leading process, the translocation of the nucleus into the leading process and the elimination of the trailing process.
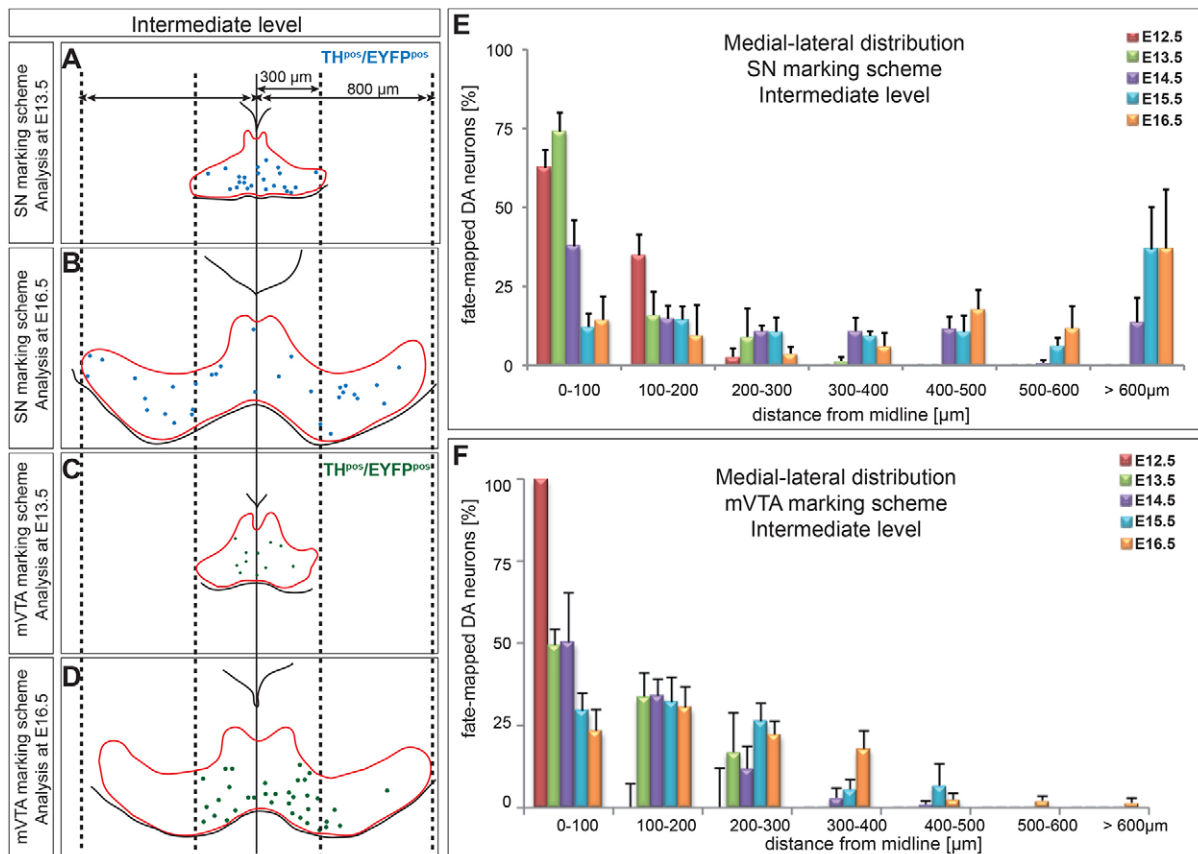
Fig. 3. DA neurons destined for the SN move laterally over time. (A-D) To-scale analysis of the distribution of DA neurons labeled with the SN or mVTA marking scheme at E13.5 and E16.5. Blue or green dots indicate fate-mapped DA neurons ($TH^{pos}/EYFP^{pos}$). Solid line, midline; dashed lines, maximum lateral position of DA neurons at E13.5 or E16.5. (E,F) Mediolateral distribution of fate-mapped DA neurons between E12.5 and E16.5 at intermediate section levels. (E) SN marking scheme: the medial (0-100 μm) to lateral (≥600 μm) shift in distribution of labeled DA neurons is highly significant ($P<0.001$) between E12.5 and E15.5 and between E12.5 and E16.5. (F) mVTA marking scheme: labeled DA neurons remain in a medial area. The change in distribution is only significant for the shift from most medial (0-100 μm) to off-medial positions (100-200 μm) between E12.5 and the subsequent stages ($P<0.001$). Note that only few $TH^{pos}/EYFP^{pos}$ cells can be detected at E12.5. Data are presented as ± s.e.m., $n=3$. Statistical significance determined by ANOVA and post-hoc Bonferroni analysis.

The leading process selects the orientation of migrating neurons in response to chemotactic cues in the environment and its orientation can serve as an indicator for the direction of migration (Marín et al., 2010; Rakic, 1990). In midbrain sections, the morphology of $TH^{pos}/EYFP^{pos}$ neurons labeled with the SN marking scheme indicated that the lateral displacement of DA neurons correlated with tangentially oriented leading processes, whereas cells labeled with the mVTA marking scheme had primarily radially oriented processes (supplementary material Fig. S3). To investigate the morphology of fate-mapped DA neurons ($TH^{pos}/EYFP^{pos}$) more precisely, we used ultramicroscopy. Ultramicroscopy allows fast multidimensional imaging of entire tissues with minimal photo-bleaching and good optical resolution. Cleared whole-mount brains immunostained for TH and EYFP were imaged (Fig. 4; supplementary material Fig. S4). Analysis of the acquired image stacks reconstructed in 3D showed that most DA neurons had a unipolar or bipolar morphology (Fig. 4B,D,F,H). DA neurons labeled with the SN marking scheme displayed radially oriented processes when located close to the ventricular zone, but tangentially oriented processes after reaching the mantle layer (Fig. 4A-D,G). By contrast, DA neurons labeled with the mVTA marking scheme had predominantly radially oriented processes and only few tangentially oriented processes (six out of 72 cells)

(Fig. 4E-G). Classification of the processes into trailing processes (radially oriented towards ventricular zone or tangentially oriented towards midline) and leading processes (radially oriented towards pial surface or tangentially oriented away from midline) showed that neurons labeled with both marking schemes had leading and trailing processes (Fig. 4H). These results support a model in which DA neurons labeled with the SN marking scheme initially undergo radial migration to reach the mantle layer and subsequently switch to tangential migration to form the SN. By contrast, neurons giving rise to the mVTA have almost exclusively radial leading/trailing processes, consistent with a predominantly radial mode of migration.

Time-lapse imaging demonstrates distinct migratory routes for DA neurons destined for the SN or medial VTA

To examine the migratory behavior of neurons labeled with the SN or mVTA marking scheme in real time, we monitored the migration of fluorescently marked cells in organotypic slice cultures using time-lapse imaging (Fig. 5). E12.5 brain slices were cultured for one day and then subjected to time-lapse imaging for 8-15 hours (Fig. 5; supplementary material Table S1). Imaging of cells labeled with the SN or mVTA marking scheme in sagittal slices showed that they follow a radial migration path (Fig. 5D; supplementary material Movies 1, 2). Cells labeled with the SN marking scheme underwent

Development
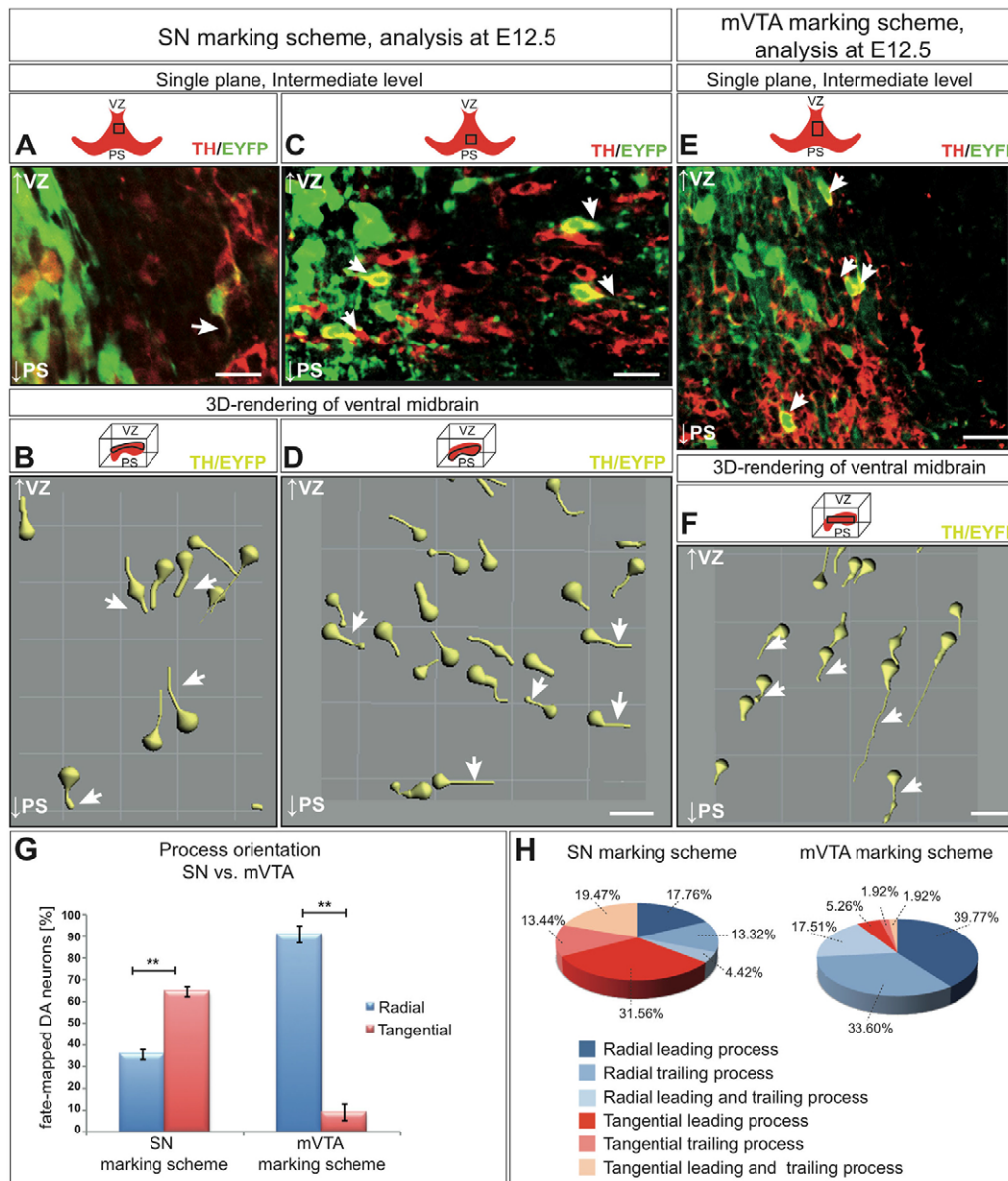
Fig. 4. DA neurons destined for the SN have tangentially oriented processes. Ultramicroscopy reveals the morphology of fate-mapped DA neurons. (A,C,E) Single plane of a 3D reconstruction of the ventral midbrain immunostained for TH and EYFP. Arrows indicate processes of fate-mapped DA neurons (TH[pos]/EYFP[pos]). PS, pial surface; VZ, ventricular zone. Schematic (red) shows the intermediate level of the DA neuronal field; box indicates where analysis was performed. (B,D,F) Fate-mapped DA neurons were traced in 3D reconstructions; a maximum intensity projection is shown. Arrows indicate tangentially oriented (D) or radially oriented (B,F) processes. Schematic (red) shows the entire DA neuronal field in 3D; outline indicates where analysis was performed. (G) Quantification of process orientation. Data are presented as ± s.e.m., n=3 embryos. **P<0.01 by unpaired Student's t-test. (H) Classification of neuronal process orientation into trailing (radially oriented towards VZ or tangentially oriented towards midline) and leading (radially oriented towards pial surface or tangentially oriented away from midline) processes. Scale bars: 100 µm.

tangential migration in horizontal slices (Fig. 5G; supplementary material Movie 3). During tangential migration, soma translocation followed the extension of a leading process (Fig. 5C; supplementary material Movie 3). Cells in which processes could be assessed in detail (n=10) had transient trailing processes (5/10 cells) and made short backward movements (3/10 cells). In addition, some tangentially migrating neurons underwent a phase of active forward movement followed by a resting period (4/10 cells). By contrast, cells labeled with the mVTA marking scheme rarely underwent tangential migration in E12.5 horizontal slices (supplementary material Movie 4). Because mVTA neurons are born later than SN neurons, their lateral movement might occur later. To assess this possibility, we examined the migration of cells labeled with the mVTA marking scheme in E13.5 and E14.5 horizontal slices, but observed only very few tangentially migrating cells (supplementary material Movies 5, 6). These data demonstrate that neurons that contribute to the SN undergo radial and tangential migration, whereas neurons destined for the mVTA primarily follow a radial migration route.

Reelin signaling regulates tangential migration of DA neurons destined for the SN

Because DA neurons destined for the SN undergo tangential migration over long distances, molecular mechanisms specifically guiding laterally migrating DA neurons should exist. The reelin pathway could play a role in regulating tangential migration of DA neurons, as it has been reported that the SN does not form in *Reeler* mutants (Kang et al., 2010; Nishikawa et al., 2003; Trommsdorff et al., 1999). Reelin, a large extracellular glycoprotein, regulates migration in several brain areas and signals via the transmembrane receptors APOER2 (APOE receptor 2; LRP8 – Mouse Genome Informatics) and VLDLR (very low density lipoprotein receptor) and the downstream effector DAB1 (disabled 1) (D'Arcangelo et al., 1999; Rice et al., 1998).

We first examined whether components of the reelin signaling pathway are specifically expressed in DA neurons that undergo tangential migration. RNA *in situ* hybridization at E13.5 showed that *Vldlr* and *Apoer2* were expressed at low levels throughout the region containing DA neurons (Fig. 6A,B; supplementary material Fig.
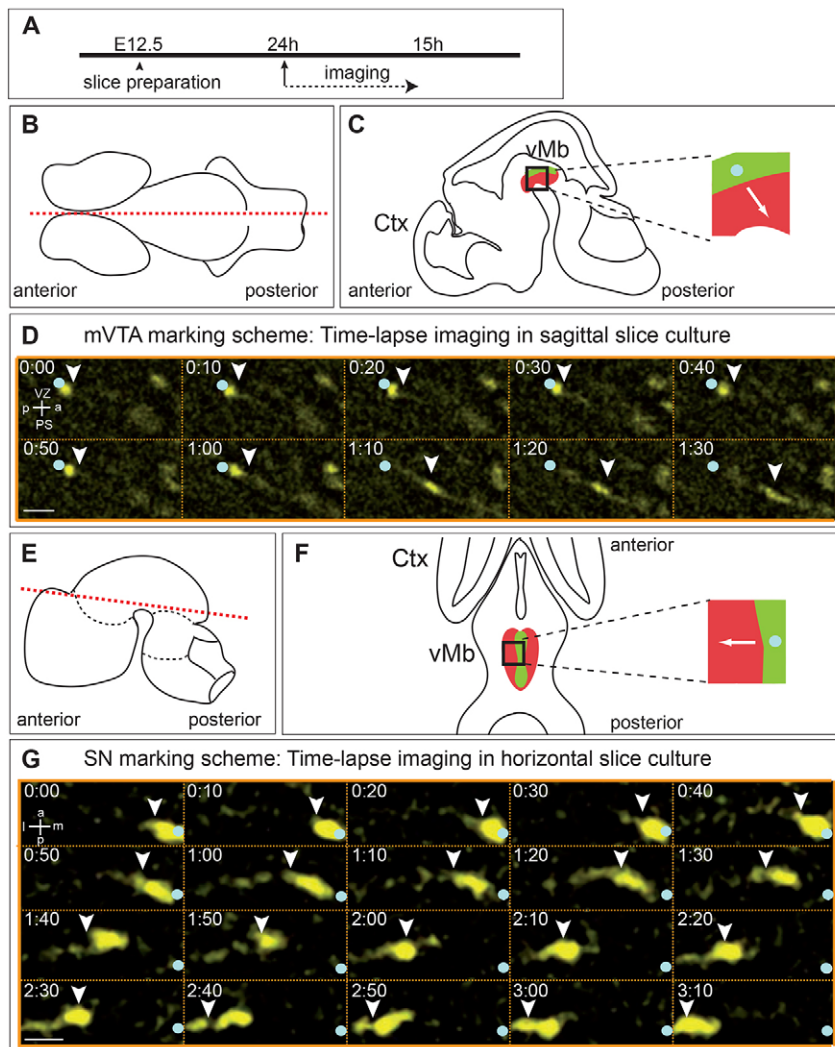
Fig. 5. DA neurons destined for the SN undergo tangential migration. (A) Experimental set-up for the time-lapse imaging in organotypic slice cultures. (B,E) Section plane for sagittal (B) and horizontal (E) slices. (C,F) The migratory path (arrow) of DA neurons from their initial position (blue dot) in the progenitor domain (green). Red area, differentiated DA neurons. Ctx, cortex; vMb, ventral midbrain. (D,G) Time-lapse imaging of EYFP^{pos} cells after 1 day *in vitro*. Images were taken every 10 minutes. E12.5 sagittal (D) or horizontal (G) slice. (D) mVTA marking scheme. The cell migrates radially (arrowhead) from its initial position (light blue dot). (G) SN marking scheme. The cell migrates laterally (arrowhead) from its initial position (light blue dot). See schematic in C or F for the imaged area. a, anterior; l, lateral; m, midline; p, posterior. Scale bars: 12.5 μm.

S5A,B). By contrast, *Dab1* expression was largely restricted to the area where tangentially migrating DA neurons contributing to the SN are located (Fig. 6C; supplementary material Fig. S5C,E-J). *Reelin* was expressed dorsally to *Dab1*-expressing cells, in an area positive for the red nucleus marker POU4F1 (POU domain, class 4, transcription factor 1) (Fig. 6D; supplementary material Fig. S5D).

To investigate whether reelin signaling is indeed required for the tangential migration of SN neurons, we inhibited reelin function in slice cultures using the function-blocking antibody CR50 (Utsunomiya-Tate et al., 2000). We monitored the migratory behavior of cells fluorescently labeled with the SN marking scheme using time-lapse imaging (Fig. 6E-I; supplementary material Fig. S5K and Table S1). Inhibition of reelin signaling led to a significant reduction in the speed of tangentially migrating cells (Fig. 6F). This effect was specific, as treatment with reelin function-blocking antibody did not alter the speed of radially migrating cells labeled with the mVTA or SN marking scheme (Fig. 6G; supplementary material Fig. S5K and Table S1). Analysis of the trajectories of tangentially migrating EYFP^{pos} cells (Fig. 6H,I) showed that reelin inhibition resulted in a significant deviation of migrating neurons (*n*=46) from the tangential trajectory compared with neurons in control slices (*n*=33) (Fig. 6I). As the leading process plays an important role in directing neuronal migration, we analyzed the morphology of TH^{pos} DA neurons in E13.5 wild-type and *Reeler*

mutant brains. We found that in *Reeler* mutants, laterally positioned DA neurons lacked tangentially oriented processes, but formed processes that were perpendicular to the tangential plane (Fig. 6J,K).

To assess whether reelin signaling in DA neurons is indeed mediated by VLDLR/APOER2 and DAB1, we examined the midbrain phenotypes of *Reeler* mutant, *Dab1* knockout (KO) or *Apoer2*/*Vldlr* double KO mice at postnatal day 25. In both *Dab1* and *Apoer2*/*Vldlr* KO mice, the SN did not extend laterally at intermediate levels and DA neurons appeared to accumulate in the VTA region, a phenotype comparable to *Reeler* mutant mice (supplementary material Fig. S6A-D). At anterior levels, however, the SN formed, but was disorganized (supplementary material Fig. S6M-P). Immunostaining for GIRK2 (G protein-gated inwardly rectifying potassium channel 2; KCNJ6 – Mouse Genome Informatics) and calbindin which are predominantly expressed in either the SN or the VTA, respectively, showed that GIRK2^{pos} DA neurons were located laterally to calbindin^{pos} DA neurons at intermediate levels (supplementary material Fig. S6E-L) (Thompson et al., 2005).

These findings show that reelin regulates the speed, trajectories and polarization of tangentially migrating DA neurons through the VLDLR/APOER2 and DAB1 pathway. Reelin signaling is essential for the proper formation of the SN, but not for the separation of SN and VTA neurons.
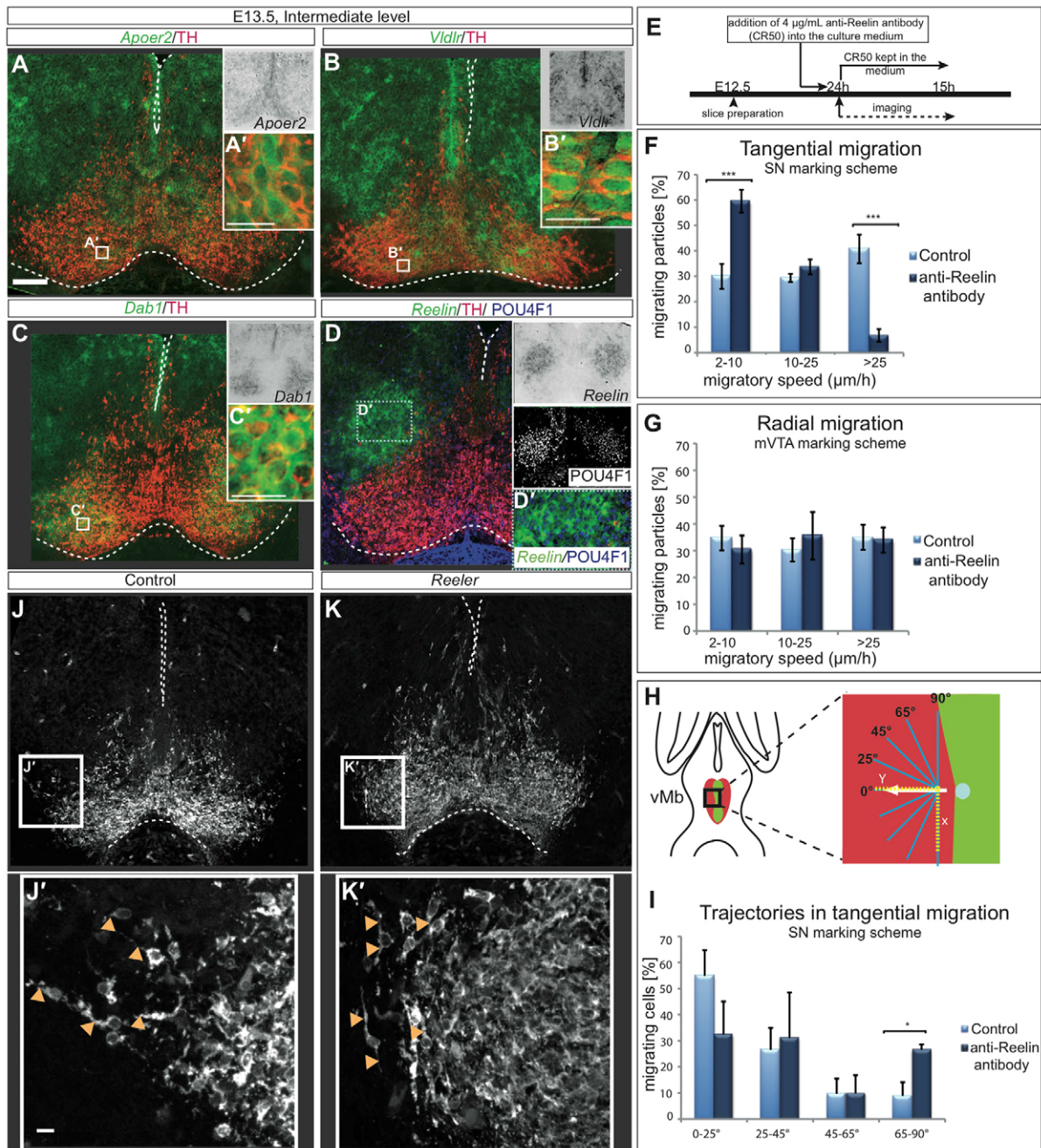
Fig. 6. Tangential migration of SN DA neurons is mediated by reelin signaling. (A-D) RNA *in situ* hybridization for components of the reelin signaling pathway. (A,B) *Apoer2* and *Vldlr* are broadly expressed in DA neurons. (C) *Dab1* is specifically expressed in the lateral DA population. (D) *Reelin* expression overlaps with the red nucleus marker, POU4F1 (immunohistochemistry). Insets are of brightfield images; inset in D also shows POU4F1 staining. (A′-D′) Higher magnifications of the boxed areas in A-D, respectively. (E) Inhibition of reelin in slice cultures. (F,G) Effect of reelin inhibition on the migratory speed of labeled cells in a horizontal (SN marking scheme, F) or in a sagittal slice (mVTA marking scheme, G). (H,I) Trajectories of migrating cells in treated or untreated slices. (H) In a best-fit linear trajectory, neurons migrate laterally (arrow) from their initial position (blue dot) along the *y*-axis (yellow line). The grades of deviation (blue lines) from the *y*- to *x*-axis (yellow line) were quantified. (I) Inhibition of reelin alters the trajectories of migrating cells (SN marking scheme). Data are presented as ± s.e.m., *n*≥3. ***P<0.001, *P<0.05 by unpaired Student's *t*-test. (J,K) TH immunostaining on E13.5 wild-type and *Reeler* mutant brains. (J′,K′) Higher magnification of the boxed areas. Arrowheads indicate DA neuronal processes. Scale bars: 100 μm (A-D,J,K); 20 μm (J′,K′).

CXCR4 and its ligand CXCL12 regulate the initial migration of DA neurons

The mechanisms that control the initial radial migration of DA neurons are unknown. Given that DA neurons migrate towards the ventral pial surface during their radially oriented movement, we hypothesized that an attractant expressed by the meningeal cell layer surrounding the pial surface could be important for this process. A potential candidate is the chemokine CXCL12. CXCL12 is a potent chemoattractant during neuronal migration in the forebrain and the hindbrain, where it is secreted from meningeal cells (fore- and hindbrain) or Cajal Retzius cells (forebrain). CXCL12 signals through the CXCR4 and CXCR7 (ACKR3 – Mouse Genome Informatics) receptors (Sánchez-Alcañiz et al., 2011; Wang et al., 2011).

667

We first analyzed the expression of *Cxcl12*, CXCR4 and *Cxcr7* in the ventral midbrain between E10.5 and E18.5 (Fig. 7; data not shown). CXCR4 was expressed in TH^{pos} DA neurons starting at E11.5 (Fig. 7A). At E13.5 and E15.5, CXCR4 was expressed in medially located TH^{pos} DA neurons, but also in TH^{neg} cells located below the ventricular zone (Fig. 7B,C). These TH^{neg} CXCR4^{pos} cells were positive for NURR1 (nuclear receptor related 1 protein; NR4A2 – Mouse Genome Informatics), which is expressed in differentiating DA neurons before the onset of TH expression, and for LMX1A, a marker for DA progenitors and differentiated DA neurons (Fig. 7E,F) (Andersson et al., 2006; Zetterström et al., 1996). CXCR4 expression levels appeared to be slightly downregulated in cells located close to the pial surface (Fig. 7B,C,E,F). By E18.5, CXCR4 could no longer be detected in the ventral midbrain (Fig. 7D). By contrast, *Cxcr7* was only expressed in the ventricular zone (Fig. 7G). *Cxcl12* mRNA was expressed in the meningeal cell layer at the time of DA neuronal migration (Fig. 7H,I).

The restricted spatial and temporal expression of CXCR4 in medially located DA neurons suggested that CXCL12/CXCR4 signaling might play a specific role in regulating the initial radial migration of DA neurons. To investigate this, we analyzed the distribution of DA neurons at E14.5 and E16.5 in mice in which *Cxcr4* (*Cxcr4* KO) or *Cxcl12* (*Cxcl12* KO) were inactivated. Postnatal stages could not be analyzed because the mice die perinatally (Ma et al., 1998; Nagasawa et al., 1996). At intermediate and posterior levels, we observed ectopic TH^{pos} DA neurons dorsal to the DA neuronal field in the mutant embryos (Fig. 8A-C; data not shown). In addition, the morphology of the cells in this area was altered in posterior sections of *Cxcl12* and *Cxcr4* KO mutants at

E16.5 (Fig. 8G-I). To quantify the change in cell distribution, ventral midbrain sections of *Cxcl12* KO, *Cxcr4* KO and wild-type embryos were divided into bins along the dorsoventral and mediolateral axis (Fig. 8D,J; see also Materials and Methods). The number of DA neurons was counted in each bin and normalized for the total number of counted DA neurons. This analysis confirmed the increased accumulation of DA neurons in the dorsal, off-midline area of the DA neuronal field in E14.5 *Cxcl12* KO and *Cxcr4* KO embryos and in E16.5 *Cxcr4* KO embryos (Fig. 8E,K). In *Cxcl12* KO mutants, the increase in dorsally located DA neurons was accompanied by a slight decrease in DA neurons in ventral, off-midline positions (Fig. 8F). By contrast, in *Cxcr4* KO embryos, DA neurons were decreased along the midline and increased in ventral, off-midline positions (Fig. 8E,F,L).

The altered distribution of DA neurons in *Cxcr4* or *Cxcl12* KO mice could be caused by changes in the speed and/or trajectories of migrating DA neurons, two aspects of migration that can be quantified in organotypic slice cultures. To this end, we inhibited CXCL12/CXCR4 signaling by adding the CXCR4 antagonist AMD3100 to the slice cultures and monitored the migration of cells labeled with the mVTA or SN marking scheme (supplementary material Fig. S7A-C and Table S1). To confirm that the antagonist abolishes CXCR4 signaling, we assessed the phosphorylation of CXCR4, which serves an indicator for CXCR4 activation (Busillo et al., 2010). We could show that phosphorylated CXCR4 is present in untreated, but not in antagonist-treated slice cultures, demonstrating that the antagonist inhibits CXCL12/CXCR4 signaling in our experimental setup (supplementary material Fig. S7D,E). However, neither the speed nor the trajectories of migrating cells was changed in cultures treated with the CXCR4 antagonist
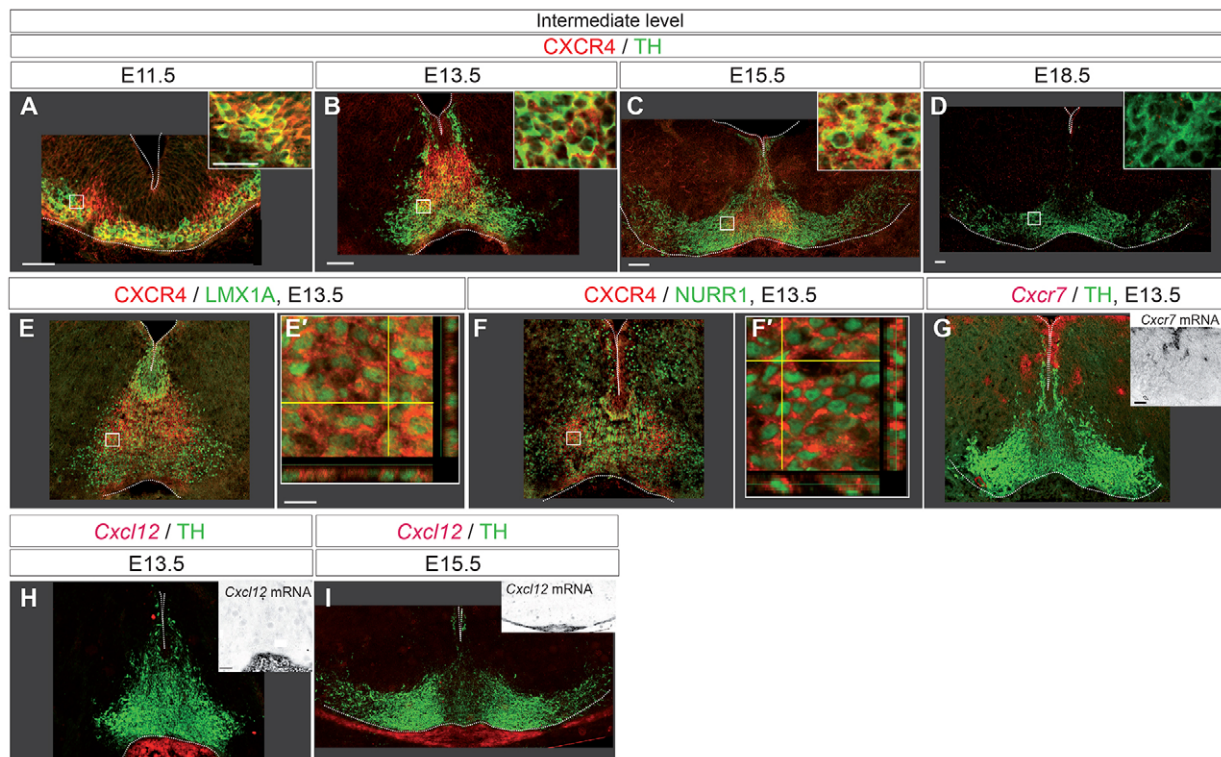
Fig. 7. CXCR4 is specifically expressed in medially located DA neurons. (A-D) Immunohistochemistry for CXCR4 and TH. Insets show higher magnifications of the boxed areas. (E-F′) Immunohistochemistry for CXCR4 and LMX1A (E) or CXCR4 and NURR1 (F). Orthogonal views within confocal *z*-stacks show LMX1A (E′) and NURR1 (F′) positive nuclei surrounded by CXCR4 protein. (G-I) Immunohistochemistry for TH and RNA *in situ* hybridization for *Cxcr7* (G) or *Cxcl12* (H,I). *Cxcr7* is not expressed in DA neurons. *Cxcl12* is expressed in the meningeal cell layer. Insets show brightfield images. Scale bars: 100 μm (A-I); 10 μm (E′,F′).
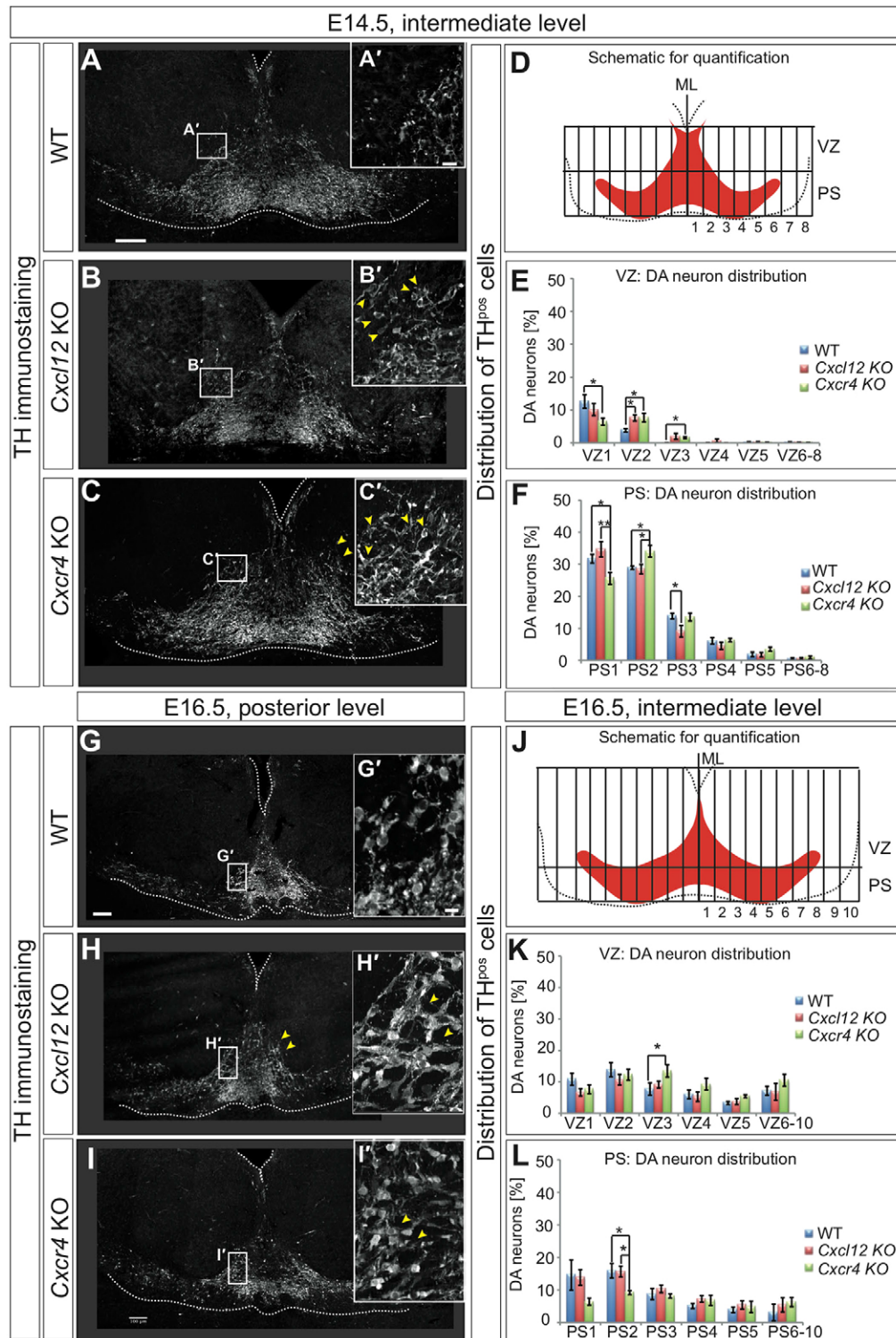
Fig. 8. CXCL12 signaling modulates the migration of DA neurons. (A-C,G-I) Immunohistochemistry for TH. Abnormal distribution of DA neurons in *Cxcl12* and *Cxcr4* KO brains. Yellow arrowheads indicate ectopic DA neurons. Scale bars: 100 μm. (A′-C′,G′-I′) Higher magnification of the boxed areas. Scale bars: 20 μm. (D-F,J-L) Quantification of the distribution of TH^{pos} cells in E14.5 and E16.5 WT, *Cxcl12* KO and *Cxcr4* KO brains. Schematics in D and J show the regions divided into a different number of bins to account for the size difference between the two stages. ML, midline; PS, pial surface; VZ, ventricular zone. DA neurons accumulate in the dorsal, off-midline area of the DA neuronal field in E14.5 *Cxcl12* KO and *Cxcr4* KO embryos (in E: VZ2, VZ3) and in E16.5 *Cxcr4* KO embryos (in K: VZ3). DA neurons are decreased in ventral, off-midline positions in *Cxcl12* KO mutants (in F: PS3). In *Cxcr4* KO embryos, DA neurons are decreased along the midline (in E: VZ1; in F: PS1; in L: PS1, PS2) and increased in ventral, off-midline positions (in F: PS2). Data are presented as ± s.e.m., *n*=4. Statistical significance determined by ANOVA and post-hoc LSD analysis, *P<0.05, **P<0.01.

(supplementary material Fig. S7A-C; data not shown), suggesting that other aspects of migration are altered in the absence of CXCR4/CXCL12 signaling (see Discussion).

DISCUSSION
Migratory paths of DA neurons
Previous attempts to characterize the migratory routes of DA neurons using birthdating and/or TH immunostaining of ventral midbrain progenitors have produced contradictory results. Thus,

several potential migratory paths have been proposed for neurons that form the SN (see Introduction) (Hanaway et al., 1971; Kawano et al., 1995; Shults et al., 1990; Vasudevan et al., 2012).

Our data show that DA neurons destined for the mVTA and SN undergo an initial radially oriented migration from the ventricular zone to the mantle layer. Radial migration of DA neurons probably occurs along densely packed radial glia fibers that extend from the ventricular zone to the mantle layer in the ventral midbrain. DA neurons are aligned along these radial processes and disruption of

radial glia results in impaired migration of DA neurons (Kawano et al., 1995; Shults et al., 1990; Tang et al., 2009).

Following this initial migration step, neurons contributing to the SN switch their migratory direction and move laterally. We demonstrate that future SN neurons undergo active tangential migration rather than being displaced laterally by newly generated medial cells or the overall growth of the tissue. Axonal processes originating from cell bodies in the ventrolateral midbrain and running along the mediolateral axis of the ventral midbrain could function as a scaffold for tangentially migrating neurons (Kawano et al., 1995).

The switch of SN neurons from radial to tangential migration is most obvious at intermediate anteroposterior levels of the developing DA neuronal field, where both SN and VTA are formed. DA neurons destined for the anterior SN assume relative lateral positions immediately after their radial migration, but our analysis of the mediolateral cell distribution shows that tangential migration also contributes to their final lateral position. At posterior levels, we only observed a few labeled DA neurons in lateral positions with the SN marking scheme. Therefore, we cannot draw any conclusion about the migratory behavior of cells giving rise to the RRF.

Reelin regulates tangential migration of DA neurons

Previous studies proposed that the SN does not form in *Reeler* mutants (Kang et al., 2010; Nishikawa et al., 2003). We show here that in *Reeler* as well as in *Dab1* KO and *Apoer2/Vldlr* double KO mutants, the lack of lateral dispersion of SN neurons is confined to intermediate levels, whereas the anterior SN is merely disorganized (see also Sharaf et al., 2013). We further demonstrate that reelin regulates the tangential migration of DA neurons by regulating their speed, trajectories and leading process orientation. These effects of reelin are consistent with some of its proposed functions during the migration of cortical projection neurons and cerebellar Purkinje cells (Britto et al., 2013; Miyata et al., 2010). Interestingly, in reelin pathway mutants, GIRK2^{pos} (primarily SN) and calbindin^{pos} (primarily VTA) neurons are still largely split into lateral and medial clusters, respectively, indicating that reelin is not required for separating the two cell populations. These data suggest that reelin is not important for the initial steps of tangential migration of SN neurons (including the switch from radial to tangential migration), but rather regulates the final tangential migration that allows SN neurons to reach their correct position in the ventrolateral midbrain (Fig. 9).

Reelin could regulate the speed and trajectories of laterally migrating DA neurons directly by acting as a chemoattractant for DA neurons. In the cortex, it has been shown that reelin, a large extracellular matrix molecule, is cleaved into smaller fragments that could potentially diffuse and build a chemoattractive gradient (Jossin et al., 2004; Lambert de Rouvroit et al., 1999). Whether reelin is similarly processed in the ventral midbrain remains to be examined.

Alternatively, reelin might be a permissive factor allowing tangentially migrating DA neurons to respond to other, still unknown, attractant molecules. Several lines of evidence support such a scenario. First, the *Reelin* mRNA expression domain, which overlaps with the red nucleus, is located dorsally rather than laterally to tangentially migrating, *Dab1*-expressing DA neurons. Second, it has been previously reported that reelin protein can be detected throughout the SN, where it might be secreted by incoming projections from striatal neurons (Nishikawa et al., 2003). Such a ubiquitous distribution of reelin would make it unlikely that reelin itself acts as a chemoattractive factor. Third, we show that reelin is important for the proper orientation of the leading processes of
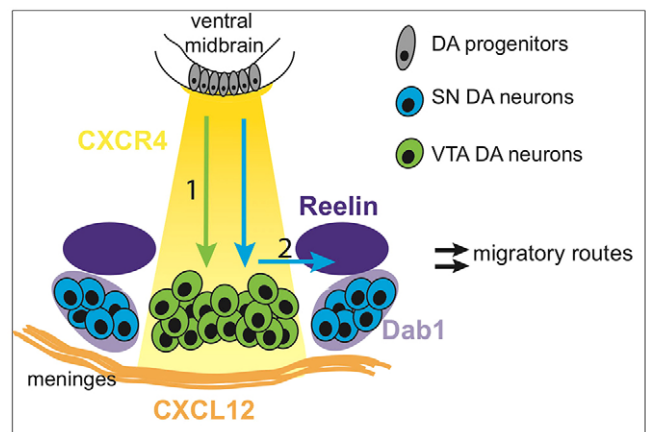
Fig. 9. Reelin and CXCL12/CXCR4 signaling modulate distinct migratory behaviors of DA neurons. CXCL12 is expressed in meninges (orange), CXCR4 is expressed in differentiating DA neurons in the medial-ventral midbrain (yellow gradient). CXCL12/CXCR4 signaling modulates the initial radial migration (1) of all DA neurons. *Reelin* (purple) is expressed dorsal to laterally migrating *Dab1*-expressing (light purple) DA neurons. Reelin regulates the tangential migration of DA neurons (2).

laterally migrating DA neurons. The dramatic misorientation of the leading processes of DA neurons in *Reeler* mutants could interfere with the ability of the DA neurons to respond to attractive cues in their environment.

CXCL12/CXCR4 signaling modulates the initial migration step of DA neurons

DA neurons that leave their progenitor domain and move radially towards the mantle layer express CXCR4, the receptor for the chemokine CXCL12. *Cxcl12* is expressed in the meninges surrounding the forming mantle layer. In both, *Cxcr4*- and *Cxcl12*-deficient mice, we observed an accumulation of DA neurons in the dorsal, off-midline area of the DA neuronal field. The accompanying reduction in ventrally positioned cells in *Cxcl12* mutants as well as the lack of expression of CXCR4 in laterally positioned DA neurons suggest a role for CXCR4/CXCL12 signaling in radial migration (Fig. 9). These results are consistent with a recently published study (Yang et al., 2013). However, we observed fewer DA neurons along the ventral midline of *Cxcr4* mutants, indicating a more complicated effect of CXCR4 signaling on DA neuronal migration. Moreover, the phenotype in both KO mice appears to be transient, suggesting that CXCL12/CXCR4 signaling is not essential for DA neuronal migration, but rather regulates the efficiency of migration. As CXCL12 is the only known ligand for CXCR4, it is surprising that the *Cxcr4* and *Cxcl12* KOs have distinct phenotypes. CXCL12-independent functions of CXCR4 have not been demonstrated, but it has been recently shown that the neurotransmitter GABA directly binds CXCR4 and can act as an allosteric modulator (Guyon et al., 2013). Whether GABA or other potential modulators could influence CXCR4 function in the absence of CXCL12 in the ventral midbrain remains to be explored.

It is unclear which aspect of DA neuronal migration is regulated by CXCL12/CXCR4 signaling. Recently, it has been reported that the process orientation of MbDN is altered in *Cxcr4* KO mice (Yang et al., 2013). However, upon inhibiting CXCL12/CXCR4 signaling in our organotypic slice cultures neither the speed nor the trajectory of radially migrating cells was significantly changed. Other changes that might account for the ectopic accumulation of DA neurons in

Cxcl12- or *Cxcr4*-deficient mice, such as premature cessation or a delayed onset of radial migration, could not be assessed in the slice cultures. Premature cessation of migration upon CXCR4 inactivation has been reported for migrating sympathetic precursor cells in the chick (Kasemeier-Kulesa et al., 2010).

CXCL12 is thought to act as a paracrine signal for migrating neurons (Stumm and Höllt, 2007; Stumm et al., 2003). A paracrine action of CXCL12 seems unlikely in migrating DA neurons, because CXCL12 is expressed in the meninges whereas most CXCR4-expressing DA neurons are located within some distance of the pial surface. Alternatively, CXCL12 might act as a long-range attractive signal for DA neurons. Previous findings show that CXCL12 is an attractant for radially migrating granule cells in the dentate gyrus and can act as a chemotactic factor for dissociated neurons *in vitro* (Bagri et al., 2002; Hesselgesser et al., 1997; Klein et al., 2001).

Conclusion

Here we characterize in detail the migratory paths taken by DA neurons that ultimately give rise to the SN or the mVTA. We demonstrate that neurons destined for the mVTA undergo radial migration to reach their final position in the ventral midbrain. By contrast, the migration of neurons giving rise to the SN consists of several steps: an initial radial migration is followed by active tangential migration resulting in the separation of SN and mVTA neurons and the formation of the SN in the lateral midbrain. We further show that reelin mediates the tangential migration that results in the final lateral position of SN. Finally, we provide evidence that the migration of DA neurons from their progenitor zone to the mantle layer is modulated by CXCR4/CXCL12 signaling.

MATERIALS AND METHODS
Mouse lines and genetic inducible fate mapping
Reeler mutants, *Apoer2, Vldlr, Dab1, Cxcr4* and *Cxcl12* knockout mice and genotyping protocols have been described previously (D'Arcangelo et al., 1995; Frykman et al., 1995; Howell et al., 1997; Ma et al., 1998; Nagasawa et al., 1996; Trommsdorff et al., 1999). *ROSA^{loxP-STOP-loxP-EYFP}* (*R26^{EYFP}*) mice were kindly provided by Dr Costantini (Srinivas et al., 2001); *Shh^{CreER}* mice were kindly provided by Dr Tabin (Harfe et al., 2004). Genotyping protocols for the *R26^{EYFP}* allele and the *CreER* alleles were previously described (Kimmel et al., 2000; Soriano, 1999). *Shh^{CreER}* and *R26^{EYFP}* mice were maintained in an outbred CD1 background. Noon of the day a vaginal plug was detected was designated as E0.5. Tamoxifen (TM, 20 mg/ml) (Sigma-Aldrich) was dissolved in corn oil (Sigma-Aldrich). To reduce miscarriages, 5 mg/ml progesterone (Sigma-Aldrich) was added. Pregnant females were given 3-4 mg TM by oral gavage with animal feeding needles (Fine Science Tools) at 12 pm of E8.5 or E11.5. Animal studies were approved by the University of Bonn Animal Care and Use Committee.

Organotypic slice cultures
Organotypic slice cultures were prepared as described previously (Bodea and Blaess, 2012). After sectioning, slices were incubated for 24 hours before being imaged. Time-lapse imaging was performed at 100× magnification at 10-minute intervals for 8-15 hours on a Zeiss Axio-Observer inverted microscope fitted with an environmental chamber at 37°C, 5% CO_2. Anti-reelin antibody (CR-50, 4 µg/ml, MBL) in 50% glycerol/PBS (Utsunomiya-Tate et al., 2000) was added to inhibit reelin signaling; 50% glycerol/PBS alone was added as control. The CXCR4 antagonist AMD3100 was diluted in culture medium (120 µM, Sigma-Aldrich) (Lysko et al., 2011). The compounds were added to the slices right before imaging was started and kept in medium during the entire imaging time.

Immunohistochemistry and *in situ* hybridization
Heads or brains were dissected, fixed in 4% paraformaldehyde (PFA) for 30-120 minutes and either embedded in Tissue-Tek OCT (Sakura) for

cryosectioning (12 µm sections) or processed for paraffin embedding (7 µm sections). For staining with anti-phosphorylated CXCR4, slice cultures were fixed in 4% PFA for 15 minutes and embedded in Tissue-Tek OCT (Sakura) for cryosectioning (12 µm sections). *In situ* hybridization and immunostaining were performed using standard procedures (Blaess et al., 2011). Plasmids containing reelin, *Dab1*, *Vldlr* and *Apoer2* cDNA were kindly provided by Dr F. Tissir (Jossin et al., 2003). RNA probes for *Cxcl12* and *Cxcr7* have been described (Sánchez-Alcañiz et al., 2011; Stumm et al., 2003).

Primary antibodies used for immunostaining were: rabbit or mouse anti-TH (1:500, AB152 or MAB318, Millipore), rat anti-GFP (1:1500, 04404-26, Nacalai Tesque), rabbit anti-LMX1A (1:3000, AB10533, Millipore), rabbit anti-NURR1 (1:200, Sc-990, Santa Cruz Biotechnology), mouse anti-POU4F1 (1:50, Sc-8429, Santa Cruz Biotechnology), rabbit anti-calbindin (1:2500, CB38, Swant), rabbit anti-GIRK2 (1:500, APC-006, Alomone Labs), biotinylated rabbit anti-CXCR4 (1:500, AB097, BD Biosciences), anti-phosphorylated CXCR4 [1:250, kindly provided by Dr Benovic (Busillo et al., 2010)]. Secondary antibodies were: donkey anti-rabbit IgG-Alexa 488 (1:500; Life Technologies), donkey anti-mouse or -rabbit Cy3 (1:200, Jackson ImmunoResearch), donkey anti-rat IgG-DyLight 488 or 647 (1:100, Jackson ImmunoResearch). For the detection of CXCR4 Cy3-labeled streptavidin was used (1:1000, Jackson ImmunoResearch). For combined RNA *in situ* hybridization and immunostaining, protocols were modified according to Eisenstat et al. (Eisenstat et al., 1999) and can be provided on request.

Images were acquired using a Zeiss AxioObserver Z1 inverted microscope with an ApoTome set-up at 200× magnification or an Olympus IX81 confocal microscope at 400× magnification. To present the RNA *in situ* hybridization and immunofluorescence signal in one image, brightfield images of the RNA *in situ* hybridization signal were assigned to a RGB channel in Axiovision software; the channel was then inverted in Adobe Photoshop.

Ultramicroscopy
Preparation of specimens and clearing
E12.5 brains were fixed in 4% PFA for 30 minutes, stained with primary (48 hours) and secondary (24 hours) antibodies, dehydrated in a graded ethanol series, placed in hexane for 1 hour and then incubated in a clearing solution of 1:2 benzylalcohol:benzylbenzoat (Sigma-Aldrich) for 48 hours at room temperature [modified from Dodt et al. (Dodt et al., 2007)].

Imaging
Optically sectioned volumetric imaging was performed using a light-sheet microscope based on an inverted microscope (TI-Eclipse, Nikon Instruments). Cleared specimens were placed in a custom-made sample cuvette (Hellma) filled with clearing solution and illuminated by a thin light-sheet (thickness w_0=2-6 µm, width 700 µm) (Ritter et al., 2010). Fluorescence was collected orthogonal to the excitation light-sheet by either a 10× or 20× air objective (CFI Plan Fluor, Nikon) and imaged onto a scientific grade CMOS camera (Orca Flash 4.0, Hamamatsu) using either a standard or additional 1.5× magnification tube lens. 3D image stacks were acquired by moving the sample through the light-sheet in steps of 1 µm with a motorized sample stage (Physik Instrumente). The detection objective was placed on a piezo-driven mount (Physik Instrumente) to compensate for focal shift due to the refractive index mismatch between clearing solution (n_{BABB}=1.56) and immersion medium (n_{air}=1.00). The displacement of the objective was coupled linearly to the motion of the sample stage such that $\Delta z_{PIFOC}=(1-n_{air}/n_{BABB})*\Delta z_{Stage}$ [similar to equation 1 in Silvestri et al. (Silvestri et al., 2012)].

Image processing
When a thin light-sheet was used, the Rayleigh length $x_R=\pi w_0^2 n/\lambda$ was smaller than the image field x_I. Out-of-focus light reducing contrast at the edges of the image was computationally removed by subtracting a minimum projection running over $P \geq x_I/2x_R$ adjacent frames. To preserve optical sectioning over the entire image field, p image stacks of the same sample volume were acquired sequentially with the light sheet focus displaced by $2x_R$. The final image stack was created by calculating the maximum intensity

projection of all background-subtracted frames acquired in the same sample plane. Image processing was performed using MATLAB (The Mathworks) functions written for this purpose.

Quantification
Fate-mapped DA neurons
The distribution of DA neurons was quantified at three anteroposterior levels ($n \geq 3$ embryos for each time point). Sections were imaged on a Zeiss Axio Observer using the AxioVison Mosaix software. Images were acquired using a 20× LD A-Plan objective and an ApoTome set-up to assess double labeling (Zeiss). For each level, the mediolateral distribution of fate-mapped DA neurons (double-positive for TH and EYFP, TH^{pos}/EYFP^{pos}) was determined by dividing the ventral midbrain into bins of 100 μm thickness along the mediolateral axis. Statistical significance was determined using two-way ANOVA, with Bonferroni post-hoc multiple comparison test (Prism 5, GraphPad).

Migration
The velocity of moving particles (total distance traveled per time) in slice cultures was assessed using Fiji MTrack2 plugin (Schindelin et al., 2012). The average migration speed of migrating cells was 25 μm/hour, but ranged between 2 μm/hour and 40 μm/hour. Cells were divided in three speed categories, so that each category contained approximately one-third of migrating cell in the control situation: low (2-10 μm/hour), medium (10-25 μm/hour) and high speed (>25 μm/hour). The percentage of cells out of the total number of cells for each category was determined (supplementary material Table S1). Statistical significance was analyzed with unpaired Student's t-test (n=3-5 animals). Migration trajectories of EYFP^{pos} cells were manually tracked with Fiji MtrackJ plugin (Meijering et al., 2012). The midline of a horizontal slice was assigned as x-axis. The best-fit tangential path was considered as being perpendicular to the x-axis and was assigned as y-axis. The trajectory in reference to the x- and y-axes was obtained by tracking somal coordinates through the imaging sequence. Deviations from the best-fit trajectory (0°) were represented in degrees (0-90°) (supplementary material Table S1).

Cxcl12 and *Cxcr4* knockouts
The area containing TH^{pos} DA neurons was divided into two bins along the dorsoventral axis (from the ventricle to the ventral pial surface) and into eight (E14.5) or ten (E16.5) bins along the mediolateral axis (from the midline to the lateral pial surface, on either side of the midline). For each side, the number of TH^{pos} cells was determined in each bin and normalized for the total number of TH^{pos} cells (expressed as percentage) (supplementary material Table S1). To take into account TH^{pos} neurons on both sides of the midline, an average was formed between the left and the right side. Statistical significance was analyzed with one-way ANOVA and LSD post-hoc multiple comparison test (n=4; SPSS, IBM).

Ultramicroscopy
3D-volume renderings of the DA neuron-containing area were generated from image stacks at 10× magnification (Fiji-3D viewer plugin). Cell bodies and processes were traced in image stacks acquired at 30× magnification with Surpass Scene FilamentTracer (Imaris, Bitplane). Statistical significance was analyzed with unpaired Student's t-test (n=3).

References

Andersson, E., Tryggvason, U., Deng, Q., Friling, S., Alekseenko, Z., Robert, B., Perlmann, T. and Ericson, J. (2006). Identification of intrinsic determinants of midbrain dopamine neurons. *Cell* **124**, 393-405.

Ang, S. L. (2009). Foxa1 and Foxa2 transcription factors regulate differentiation of midbrain dopaminergic neurons. *Adv. Exp. Med. Biol.* **651**, 58-65.

Bagri, A., Gurney, T., He, X., Zou, Y. R., Littman, D. R., Tessier-Lavigne, M. and Pleasure, S. J. (2002). The chemokine SDF1 regulates migration of dentate granule cells. *Development* **129**, 4249-4260.

Ballmaier, M., Zoli, M., Leo, G., Agnati, L. F. and Spano, P. (2002). Preferential alterations in the mesolimbic dopamine pathway of heterozygous reeler mice: an emerging animal-based model of schizophrenia. *Eur. J. Neurosci.* **15**, 1197-1205.

Bayer, S. A., Wills, K. V., Triarhou, L. C. and Ghetti, B. (1995). Time of neuron origin and gradients of neurogenesis in midbrain dopaminergic neurons in the mouse. *Exp. Brain Res.* **105**, 191-199.

Björklund, A. and Dunnett, S. B. (2007). Dopamine neuron systems in the brain: an update. *Trends Neurosci.* **30**, 194-202.

Blaess, S., Bodea, G. O., Kabanova, A., Chanet, S., Mugniery, E., Derouiche, A., Stephen, D. and Joyner, A. L. (2011). Temporal-spatial changes in Sonic Hedgehog expression and signaling reveal different potentials of ventral mesencephalic progenitors to populate distinct ventral midbrain nuclei. *Neural Dev.* **6**, 29.

Bodea, G. O. and Blaess, S. (2012). Organotypic slice cultures of embryonic ventral midbrain: a system to study dopaminergic neuronal development in vitro. *J. Vis. Exp.* •••, e3350.

Britto, J. M., Tait, K. J., Lee, E. P., Gamble, R. S., Hattori, M. and Tan, S. S. (2013). Exogenous Reelin Modifies the Migratory Behavior of Neurons Depending on Cortical Location. *Cereb. Cortex.*

Brown, A., Machan, J. T., Hayes, L. and Zervas, M. (2011). Molecular organization and timing of Wnt1 expression define cohorts of midbrain dopamine neuron progenitors in vivo. *J. Comp. Neurol.* **519**, 2978-3000.

Busillo, J. M., Armando, S., Sengupta, R., Meucci, O., Bouvier, M. and Benovic, J. L. (2010). Site-specific phosphorylation of CXCR4 is dynamically regulated by multiple kinases and results in differential modulation of CXCR4 signaling. *J. Biol. Chem.* **285**, 7805-7817.

Chédotal, A. (2010). Should I stay or should I go? Becoming a granule cell. *Trends Neurosci.* **33**, 163-172.

Chung, S., Leung, A., Han, B. S., Chang, M. Y., Moon, J. I., Kim, C. H., Hong, S., Pruszak, J., Isacson, O. and Kim, K. S. (2009). Wnt1-lmx1a forms a novel autoregulatory loop and controls midbrain dopaminergic differentiation synergistically with the SHH-FoxA2 pathway. *Cell Stem Cell* **5**, 646-658.

D'Arcangelo, G., Miao, G. G., Chen, S. C., Soares, H. D., Morgan, J. I. and Curran, T. (1995). A protein related to extracellular matrix proteins deleted in the mouse mutant reeler. *Nature* **374**, 719-723.

D'Arcangelo, G., Homayouni, R., Keshvara, L., Rice, D. S., Sheldon, M. and Curran, T. (1999). Reelin is a ligand for lipoprotein receptors. *Neuron* **24**, 471-479.

Dailly, E., Chenu, F., Renard, C. E. and Bourin, M. (2004). Dopamine, depression and antidepressants. *Fundam. Clin. Pharmacol.* **18**, 601-607.

Demyanenko, G. P., Shibata, Y. and Maness, P. F. (2001). Altered distribution of dopaminergic neurons in the brain of L1 null mice. *Brain Res. Dev. Brain Res.* **126**, 21-30.

Dodt, H. U., Leischner, U., Schierloh, A., Jährling, N., Mauch, C. P., Deininger, K., Deussing, J. M., Eder, M., Zieglgänsberger, W. and Becker, K. (2007). Ultramicroscopy: three-dimensional visualization of neuronal networks in the whole mouse brain. *Nat. Methods* **4**, 331-336.

Eisenstat, D. D., Liu, J. K., Mione, M., Zhong, W., Yu, G., Anderson, S. A., Ghattas, I., Puelles, L. and Rubenstein, J. L. (1999). DLX-1, DLX-2, and DLX-5 expression define distinct stages of basal forebrain differentiation. *J. Comp. Neurol.* **414**, 217-237.

Frykman, P. K., Brown, M. S., Yamamoto, T., Goldstein, J. L. and Herz, J. (1995). Normal plasma lipoproteins and fertility in gene-targeted mice homozygous for a disruption in the gene encoding very low density lipoprotein receptor. *Proc. Natl. Acad. Sci. USA* **92**, 8453-8457.

Development

Guyon, A., Kussrow, A., Olmsted, I. R., Sandoz, G., Bornhop, D. J. and Nahon, J. L. (2013). Baclofen and other GABAB receptor agents are allosteric modulators of the CXCL12 chemokine receptor CXCR4. *J. Neurosci.* **33**, 11643-11654.

Hanaway, J., McConnell, J. A. and Netsky, M. G. (1971). Histogenesis of the substantia nigra, ventral tegmental area of Tsai and interpeduncular nucleus: an autoradiographic study of the mesencephalon in the rat. *J. Comp. Neurol.* **142**, 59-73.

Harfe, B. D., Scherz, P. J., Nissim, S., Tian, H., McMahon, A. P. and Tabin, C. J. (2004). Evidence for an expansion-based temporal Shh gradient in specifying vertebrate digit identities. *Cell* **118**, 517-528.

Hayes, L., Zhang, Z., Albert, P., Zervas, M. and Ahn, S. (2011). Timing of Sonic hedgehog and Gli1 expression segregates midbrain dopamine neurons. *J. Comp. Neurol.* **519**, 3001-3018.

Hesselgesser, J., Halks-Miller, M., DelVecchio, V., Peiper, S. C., Hoxie, J., Kolson, D. L., Taub, D. and Horuk, R. (1997). CD4-independent association between HIV-1 gp120 and CXCR4: functional chemokine receptors are expressed in human neurons. *Curr. Biol.* **7**, 112-121.

Howell, B. W., Hawkes, R., Soriano, P. and Cooper, J. A. (1997). Neuronal position in the developing brain is regulated by mouse disabled-1. *Nature* **389**, 733-737.

Ikemoto, S. (2007). Dopamine reward circuitry: two projection systems from the ventral midbrain to the nucleus accumbens-olfactory tubercle complex. *Brain Res. Rev.* **56**, 27-78.

Joksimovic, M., Anderegg, A., Roy, A., Campochiaro, L., Yun, B., Kittappa, R., McKay, R. and Awatramani, R. (2009). Spatiotemporally separable Shh domains in the midbrain define distinct dopaminergic progenitor pools. *Proc. Natl. Acad. Sci. USA* **106**, 19185-19190.

Jossin, Y., Ogawa, M., Metin, C., Tissir, F. and Goffinet, A. M. (2003). Inhibition of SRC family kinases and non-classical protein kinases C induce a reeler-like malformation of cortical plate development. *J. Neurosci.* **23**, 9953-9959.

Jossin, Y., Ignatova, N., Hiesberger, T., Herz, J., Lambert de Rouvroit, C. and Goffinet, A. M. (2004). The central fragment of Reelin, generated by proteolytic processing in vivo, is critical to its function during cortical plate development. *J. Neurosci.* **24**, 514-521.

Kang, W. Y., Kim, S. S., Cho, S. K., Kim, S., Suh-Kim, H. and Lee, Y. D. (2010). Migratory defect of mesencephalic dopaminergic neurons in developing reeler mice. *Anat Cell Biol* **43**, 241-251.

Kasemeier-Kulesa, J. C., McLennan, R., Romine, M. H., Kulesa, P. M. and Lefcort, F. (2010). CXCR4 controls ventral migration of sympathetic precursor cells. *J. Neurosci.* **30**, 13078-13088.

Kawano, H., Ohyama, K., Kawamura, K. and Nagatsu, I. (1995). Migration of dopaminergic neurons in the embryonic mesencephalon of mice. *Brain Res. Dev. Brain Res.* **86**, 101-113.

Kimmel, R. A., Turnbull, D. H., Blanquet, V., Wurst, W., Loomis, C. A. and Joyner, A. L. (2000). Two lineage boundaries coordinate vertebrate apical ectodermal ridge formation. *Genes Dev.* **14**, 1377-1389.

Klein, R. S., Rubin, J. B., Gibson, H. D., DeHaan, E. N., Alvarez-Hernandez, X., Segal, R. A. and Luster, A. D. (2001). SDF-1 alpha induces chemotaxis and enhances Sonic hedgehog-induced proliferation of cerebellar granule cells. *Development* **128**, 1971-1981.

Lambert de Rouvroit, C., de Bergeyck, V., Cortvrindt, C., Bar, I., Eeckhout, Y. and Goffinet, A. M. (1999). Reelin, the extracellular matrix protein deficient in reeler mutant mice, is processed by a metalloproteinase. *Exp. Neurol.* **156**, 214-217.

Lysko, D. E., Putt, M. and Golden, J. A. (2011). SDF1 regulates leading process branching and speed of migrating interneurons. *J. Neurosci.* **31**, 1739-1745.

Ma, Q., Jones, D., Borghesani, P. R., Segal, R. A., Nagasawa, T., Kishimoto, T., Bronson, R. T. and Springer, T. A. (1998). Impaired B-lymphopoiesis, myelopoiesis, and derailed cerebellar neuron migration in CXCR4- and SDF-1-deficient mice. *Proc. Natl. Acad. Sci. USA* **95**, 9448-9453.

Marchand, R. and Poirier, L. J. (1983). Isthmic origin of neurons of the rat substantia nigra. *Neuroscience* **9**, 373-381.

Marín, O., Valiente, M., Ge, X. and Tsai, L. H. (2010). Guiding neuronal cell migrations. *Cold Spring Harb. Perspect. Biol.* **2**, a001834.

Meijering, E., Dzyubachyk, O. and Smal, I. (2012). Methods for cell and particle tracking. *Methods Enzymol.* **504**, 183-200.

Miyata, T., Ono, Y., Okamoto, M., Masaoka, M., Sakakibara, A., Kawaguchi, A., Hashimoto, M. and Ogawa, M. (2010). Migration, early axonogenesis, and Reelin-dependent layer-forming behavior of early/posterior-born Purkinje cells in the developing mouse lateral cerebellum. *Neural Dev.* **5**, 23.

Nagasawa, T., Hirota, S., Tachibana, K., Takakura, N., Nishikawa, S., Kitamura, Y., Yoshida, N., Kikutani, H. and Kishimoto, T. (1996). Defects of B-cell lymphopoiesis and bone-marrow myelopoiesis in mice lacking the CXC chemokine PBSF/SDF-1. *Nature* **382**, 635-638.

Nakatani, T., Kumai, M., Mizuhara, E., Minaki, Y. and Ono, Y. (2010). Lmx1a and Lmx1b cooperate with Foxa2 to coordinate the specification of dopaminergic neurons and control of floor plate cell differentiation in the developing mesencephalon. *Dev. Biol.* **339**, 101-113.

Nishikawa, S., Goto, S., Yamada, K., Hamasaki, T. and Ushio, Y. (2003). Lack of Reelin causes malpositioning of nigral dopaminergic neurons: evidence from comparison of normal and Reln(rl) mutant mice. *J. Comp. Neurol.* **461**, 166-173.

Rakic, P. (1990). Principles of neural cell migration. *Experientia* **46**, 882-891.

Rice, D. S., Sheldon, M., D'Arcangelo, G., Nakajima, K., Goldowitz, D. and Curran, T. (1998). Disabled-1 acts downstream of Reelin in a signaling pathway that controls laminar organization in the mammalian brain. *Development* **125**, 3719-3729.

Ritter, J. G., Veith, R., Veenendaal, A., Siebrasse, J. P. and Kubitscheck, U. (2010). Light sheet microscopy for single molecule tracking in living tissue. *PLoS ONE* **5**, e11639.

Sánchez-Alcañiz, J. A., Haege, S., Mueller, W., Pla, R., Mackay, F., Schulz, S., López-Bendito, G., Stumm, R. and Marín, O. (2011). Cxcr7 controls neuronal migration by regulating chemokine responsiveness. *Neuron* **69**, 77-90.

Schindelin, J., Arganda-Carreras, I., Frise, E., Kaynig, V., Longair, M., Pietzsch, T., Preibisch, S., Rueden, C., Saalfeld, S., Schmid, B. et al. (2012). Fiji: an open-source platform for biological-image analysis. *Nat. Methods* **9**, 676-682.

Sharaf, A., Bock, H. H., Spittau, B., Bouché, E. and Krieglstein, K. (2013). ApoER2 and VLDLr are required for mediating reelin signalling pathway for normal migration and positioning of mesencephalic dopaminergic neurons. *PLoS ONE* **8**, e71091.

Shults, C. W., Hashimoto, R., Brady, R. M. and Gage, F. H. (1990). Dopaminergic cells align along radial glia in the developing mesencephalon of the rat. *Neuroscience* **38**, 427-436.

Silvestri, L., Bria, A., Sacconi, L., Iannello, G. and Pavone, F. S. (2012). Confocal light sheet microscopy: micron-scale neuroanatomy of the entire mouse brain. *Opt. Express* **20**, 20582-20598.

Soriano, P. (1999). Generalized lacZ expression with the ROSA26 Cre reporter strain. *Nat. Genet.* **21**, 70-71.

Srinivas, S., Watanabe, T., Lin, C. S., William, C. M., Tanabe, Y., Jessell, T. M. and Costantini, F. (2001). Cre reporter strains produced by targeted insertion of EYFP and ECFP into the ROSA26 locus. *BMC Dev. Biol.* **1**, 4.

Stumm, R. and Höllt, V. (2007). CXC chemokine receptor 4 regulates neuronal migration and axonal pathfinding in the developing nervous system: implications for neuronal regeneration in the adult brain. *J. Mol. Endocrinol.* **38**, 377-382.

Stumm, R. K., Zhou, C., Ara, T., Lazarini, F., Dubois-Dalcq, M., Nagasawa, T., Höllt, V. and Schulz, S. (2003). CXCR4 regulates interneuron migration in the developing neocortex. *J. Neurosci.* **23**, 5123-5130.

Sulzer, D. (2007). Multiple hit hypotheses for dopamine neuron loss in Parkinson's disease. *Trends Neurosci.* **30**, 244-250.

Tang, M., Miyamoto, Y. and Huang, E. J. (2009). Multiple roles of beta-catenin in controlling the neurogenic niche for midbrain dopamine neurons. *Development* **136**, 2027-2038.

Thompson, L., Barraud, P., Andersson, E., Kirik, D. and Björklund, A. (2005). Identification of dopaminergic neurons of nigral and ventral tegmental area subtypes in grafts of fetal ventral mesencephalon based on cell morphology, protein expression, and efferent projections. *J. Neurosci.* **25**, 6467-6477.

Trommsdorff, M., Gotthardt, M., Hiesberger, T., Shelton, J., Stockinger, W., Nimpf, J., Hammer, R. E., Richardson, J. A. and Herz, J. (1999). Reeler/Disabled-like disruption of neuronal migration in knockout mice lacking the VLDL receptor and ApoE receptor 2. *Cell* **97**, 689-701.

Utsunomiya-Tate, N., Kubo, K., Tate, S., Kainosho, M., Katayama, E., Nakajima, K. and Mikoshiba, K. (2000). Reelin molecules assemble together to form a large protein complex, which is inhibited by the function-blocking CR-50 antibody. *Proc. Natl. Acad. Sci. USA* **97**, 9729-9734.

Vasudevan, A., Won, C., Li, S., Erdélyi, F., Szabó, G. and Kim, K. S. (2012). Dopaminergic neurons modulate GABA neuron migration in the embryonic midbrain. *Development* **139**, 3136-3141.

Wang, Y., Li, G., Stanco, A., Long, J. E., Crawford, D., Potter, G. B., Pleasure, S. J., Behrens, T. and Rubenstein, J. L. (2011). CXCR4 and CXCR7 have distinct functions in regulating interneuron migration. *Neuron* **69**, 61-76.

Winterer, G. and Weinberger, D. R. (2004). Genes, dopamine and cortical signal-to-noise ratio in schizophrenia. *Trends Neurosci.* **27**, 683-690.

Wise, R. A. (2009). Roles for nigrostriatal – not just mesocorticolimbic – dopamine in reward and addiction. *Trends Neurosci.* **32**, 517-524.

Yan, C. H., Levesque, M., Claxton, S., Johnson, R. L. and Ang, S. L. (2011). Lmx1a and lmx1b function cooperatively to regulate proliferation, specification, and differentiation of midbrain dopaminergic progenitors. *J. Neurosci.* **31**, 12413-12425.

Yang, S., Edman, L. C., Sánchez-Alcañiz, J. A., Fritz, N., Bonilla, S., Hecht, J., Uhlén, P., Pleasure, S. J., Villaescusa, J. C., Marín, O. et al. (2013). Cxcl12/Cxcr4 signaling controls the migration and process orientation of A9-A10 dopaminergic neurons. *Development* **140**, 4554-4564.

Zetterström, R. H., Williams, R., Perlmann, T. and Olson, L. (1996). Cellular expression of the immediate early transcription factors Nurr1 and NGFI-B suggests a gene regulatory role in several brain regions including the nigrostriatal dopamine system. *Brain Res. Mol. Brain Res.* **41**, 111-120.

Development